RSC Advances

PAPER

View Article Online
View Journal | View Issue

Cite this: *RSC Adv.*, 2024, **14**, 11513

In situ growth of Bi-MOF on cotton fabrics *via* ultrasonic synthesis strategy for recyclable photocatalytic textiles†

Hengjie Qin,[a] Ying Lv [b] and Koji Nakane *[a]

Received 19th January 2024
Accepted 28th March 2024

DOI: 10.1039/d4ra00493k

rsc.li/rsc-advances

Bismuth-based metal–organic framework (Bi-MOF) materials have shown potential for treating organic pollutants. In this work, multifunctional textiles were produced by *in situ* synthesis of CAU-17 on carboxymethylated cotton fabrics by solvothermal and ultrasonic strategies and employed as recyclable photocatalysts. The compositional and structural features of the dense MOF crystal coatings on cotton fibers were confirmed by scanning electron microscopy, X-ray diffraction, and other characterization approaches. Under optimized conditions, the developed functionalized cotton fabrics achieved a photodegradation efficiency of 98.8% under visible light for RhB in water, as well as good recyclability. The described results have provided the basis and reference for the fabrication of MOF-functionalized textiles.

1. Introduction

Metal–organic frameworks (MOFs) have captivated the forefront of scientific inquiry owing to their extraordinary structural diversity and extensive range of potential applications.[1] These highly porous materials emerge from the coordination of metal ions or clusters with organic ligands, endowing them with customizable pore dimensions, expansive surface areas, and versatile chemical reactivity.[2,3] Over recent years, MOFs have found diverse utility in gas adsorption,[4] energy storage,[5] separation processes,[6] and catalytic reactions,[7] and have demonstrated excellent performance. Nevertheless, a major obstacle in the practical use of MOFs is their predominantly powdered form, which is not only impractical for applications and recycling but also poses the risk of secondary pollution.[8,9] Consequently, the seamless integration of MOFs into practical applications remains a significant challenge.

Bismuth-based MOFs (Bi-MOFs) are currently experiencing heightened consideration due to the intrinsic advantages of low toxicity, cost-effectiveness, and abundant reserves associated with metallic bismuth. Leveraging the flexible coordination structure of Bi(III) cations, numerous Bi-MOFs have been documented, showcasing substantial structural diversity.[10] In addition, Bi-MOFs have been considered as a promising category of photocatalytic materials due to the tunable pore structure and abundant active sites. Nguyen *et al.*[11] have synthesized fully crystalline spherical Bi-BDC-MW by a microwave-assisted solvothermal method, with 99.44% of Rhodamine B (RhB) removed after 360 min visible LED light irradiation due to its high specific surface area, oxygen defects, and unique morphology. Wang *et al.*[12] introduced Bi-mna as a photocatalyst for the decomposition of RhB, demonstrating significant catalytic activity with a degradation rate of 95% within 2 h. A mechanism of ligand-to-ligand charge transfer was also proposed to characterize the transfer of photogenerated electrons from the S atom to the O atom of the pyridine ring. Huang *et al.*[13] synthesized $Bi_2(Hpdc)_2(pdc)_2\cdot 2H_2O$ with 1D structure using pyridine-2,6-dicarboxylic acid (H_2pdc), which could degrade 97% of RhB. In addition, α-Bi_2O_3 was prepared by using $Bi_2(Hpdc)_2(pdc)_2\cdot 2H_2O$ as a precursor, exhibited excellent catalytic performance.

Overall, numerous researches have shown that Bi-MOFs are more suitable candidates for the photocatalytic. However, further works related to the attachment of Bi-MOFs to appropriate substrate materials to enhance the stability and catalytic activity still need to be investigated. In addition, different synthesis techniques will significantly affect the growth of Bi-MOFs. The solvothermal method, a conventional approach, has been extensively employed for Bi-MOFs synthesis.[14] Nevertheless, the high-temperature and pressure synthesis environment may damage the substrate materials, thereby impacting the loading capacity of MOF particles. Therefore, the synthesis strategy with mild reaction conditions, such as ultrasonic synthesis,[15] emerges as a more propitious avenue for the practical implementation of MOFs.

Herein, a typical porous Bi-MOF (CAU-17) was selected as the research object, $Bi(NO_3)_3\cdot 5H_2O$ and 1,3,5-benzentricaboxylic

[a]*Frontier Fiber Technology and Science, University of Fukui, Bunkyo 3-9-1, Fukui, 910-8507, Japan. E-mail: nakane@matse.u-fukui.ac.jp*

[b]*New Energy College, Xi'an Shiyou University, No. 18 East Section 2nd Dianzi Road, Xi'an, 710065, China*

† Electronic supplementary information (ESI) available. See DOI: https://doi.org/10.1039/d4ra00493k

acid (H_3BTC) were employed as precursors, CAU-17 crystals with different dimensions were grown on carboxymethylated cotton fibers by solvothermal and ultrasonic methods, respectively. The structural properties of the obtained CAU-17-modified cotton fabrics were investigated by a series of characterization methods. Photocatalytic performance of prepared CAU-17-modified cotton fabrics was verified by degrading RhB under visible light, which could be easily recycled from water. Overall, we demonstrated for the first time the growth strategy of CAU-17 on cotton fabrics, offering a new thought for the expanded application of Bi-MOFs.

2. Experimental section

2.1 Materials

Sodium hydroxide (NaOH), and 2-propanol (C_3H_8O, IPA) were purchased from Nacalai Tesque, Inc. (Kyoto, Japan). 1,3,5-Benzentricaboxylic acid (H_3BTC) was obtained from Tokyo Chemical Industry Co., LTD (Tokyo, Japan). Bismuth nitrate pentahydrate ($Bi(NO_3)_3 \cdot 5H_2O$), cetyltrimethylammonium bromide (CTAB), methanol (MeOH), ethanol (EtOH), sodium chloroacetate ($ClCH_2COONa$), ethylenediaminetetraacetic acid disodium (EDTA–2Na), rhodamine B (RhB) and 1,4-benzoquinone ($C_6H_4O_2$, BQ) were purchased from Fujifilm Wako Pure Chemical Co., (Osaka, Japan). Cotton fabric (CF) was provided by Shikisensha Co., LTD (Osaka, Japan). All materials were analytical grade and used as received without further purification.

2.2 Characterization

Powder X-ray diffraction (PXRD) analyses were carried out using Rigaku Mini Flex II (Tokyo, Japan) with a Cu-Kα light source (30 kV, 15 mA). X-ray diffraction (XRD) analyses were performed on Rigaku Ultima-IV (Tokyo, Japan) which was equipped with a sample holder for the fibrous samples. Scanning electron microscopy (SEM) was performed on Keyence VE-9800 (Osaka, Japan) at 5 eV. X-ray photoelectron spectroscopy (XPS) analyzed with JEOL JPS-9010MCY (Tokyo, Japan) was performed with Mg-Kα as an X-ray source, the voltage at 12 kV, and the current at 5 mA to determine the chemical states. The spectra were calibrated by the C 1s peak from residual carbon with the binding energy of 284.8 eV. The pore structure and specific surface area of all samples were measured via N_2 adsorption–desorption isotherms on Belsorp-mini II (Osaka, Japan) at 77 K, and the specific surface areas were calculated according to the Brunauer–Emmett–Teller (BET) method and the pore size distribution was obtained by Barrett–Joyner–Halenda (BJH) model. The Fourier-transform infrared (FT-IR) spectra data were obtained at room temperature employing Shimadzu IR Affinity-1 (Kyoto, Japan) that was equipped with a single reflection ATR containing a diamond/ZnSe crystal. Thermogravimetric (TG) measurements were carried out by using Shimadzu DTG-60 (Kyoto, Japan) at a heating rate of 10 °C min^{-1} from 30 to 600 °C under air atmosphere. The absorption spectra from 450 to 650 nm were recorded using a Shimadzu UV-2450 spectrometer (Kyoto, Japan). The concentration of Bi ion was analyzed by using SPS7800 Inductively Coupled Plasma-Atomic Emission Spectroscopy (ICP-AES) (Tokyo, Japan), a certain amount of 5% nitric acid was dropped to dissolve the MOF particles before measurement due to the insolubility of Bi-MOF in water.

2.3 Synthetic methods

2.3.1 Carboxymethylation of cotton. To increase the available active sites on the surface of cotton fibers, the cotton fabrics were first modified by carboxymethylation methods to yield carboxylates. The carboxymethylation of cotton was performed as previously described[16] with some modifications. In a typical method, 5% NaOH was dissolved in a 100 mL solution in which the volume ratio of absolute ethanol to deionized water was 2 : 1. Two pieces of cleaned cotton fabrics (3 × 6 cm) were added to the solution and stirred slowly for 30 min at room temperature. Subsequently, the fabric was removed and 1 M of sodium chloroacetate was dissolved into the solution, then the fabric was put back into the solution and continued stirring for 1 h. The obtained cotton fabric was washed several times with deionized water and ethanol until the washing solution had become neutral, lastly, the fabric was dried in a vacuum drying oven at 40 °C for 6 h, and the resulting carboxymethyl cotton fabric was marked as CCF.

The concentration of carboxymethyl groups was determined by titration method.[17] 100 mg samples were treated with 50 mL of an aqueous NaOH solution (0.01 mol L^{-1}) for 2 h under constant agitation. Soon thereafter the NaOH solution was titrated with an aqueous HCl solution (0.01 mol L^{-1}) with 0.1% phenolphthalein solution as an indicator. Blank experiments were created to minimize errors. The concentration of carboxylate groups was calculated based on the following eqn (1):

$$C_{COOH} = \frac{C_{HCl}(V_B - V_S)}{m} \quad (1)$$

where C_{COOH} (mmol g^{-1}) is the carboxymethyl groups amount, and m (g) is the mass of sample. C_{HCl} (mol L^{-1}) is the concentration of HCl solution, V_B and V_S (mL) are the volume of HCl used for titration of blank solution and the sample solution, respectively.

2.3.2 Bi-based materials synthesis by solvothermal method. In a typical synthesis,[18] 750 mg H_3BTC and 150 mg $Bi(NO_3)_3 \cdot 5H_2O$ dissolved in 60 mL methanol, the solution was ultrasonicated for 5 min until transparent, then transferred to a 100 mL Teflon-lined autoclave and maintained at 120 °C for 24 h. The white product was washed three times with methanol and dried under vacuum at 60 °C overnight, denoted as CAU-17_ST (ST means solvothermal method).

For loading MOF onto cotton fabrics, during the above process, the prepared CCF (3 × 3 cm) and untreated CF were added to the precursor mixture solution prior to the solvothermal reaction, respectively. After the reaction, the cotton fabric was collected and washed by MeOH, noted as CAU-17_ST@CCF and CAU-17_ST@CF.

2.3.3 Bi-based materials synthesis by ultrasonic method. CAU-17 was synthesized by ultrasonic at room temperature

according to the reported methods with some modifications.[15] 150 mg $Bi(NO_3)_3 \cdot 5H_2O$, 750 mg H_3BTC, and the appropriate amount of CTAB were weighed and mixed with 20 mL of methanol in a 50 mL beaker and sealed with a parafilm. Subsequently, the mixed solution was ultrasonicated for 1 h by Mxmoonant yl-46 (600 W, 45 kHz). In addition, the same starting temperature (20 °C) and water volume (15 L) were used for all sample preparation processes to minimize the effects of temperature variations on samples during the use of the ultrasonic equipment. The obtained white precipitate was centrifuged and washed three times with methanol and dried under vacuum at 60 °C. The final product was labeled as CAU-17_*X* (*X* means the amount of CTAB used, mg).

Under the MOF synthesis conditions described as above, CCF and CF were added to prepare MOF composites. The composite cotton fabrics were named as CAU-17_*X*@CCF and CAU-17_*X*@CF, respectively.

2.4 Photocatalytic experiments

2.4.1 Photocatalytic degradation of RhB. The photocatalytic degradation of RhB was carried out in a 100 mL glass beaker. The reactor was illuminated by a visible light source provided by a SCHOTT MegaLight 100 with a 100 W halogen lamp. In every test, 3 × 3 cm (approximately 100 mg) of composites (or 10 mg of powdered samples) were used as photocatalysts and immersed in a 50 mL RhB solution with a concentration of 5 mg L^{-1} under dark conditions. Before irradiation, the solution was magnetically stirred in the dark for 60 min to ensure the establishment of an adsorption/desorption equilibrium between the photocatalysts and the RhB solution. Subsequently, the light was turned on and stirring was continued under light conditions for 2 h. During the degradation process, 2 mL of clarified solution was extracted from the solution every 30 min and filtered with a 0.22 μm needle filter. The concentration of RhB solution was determined by detecting the absorbance of the solution at λ = 554 nm by UV-vis spectrophotometer. The photodegradation efficiency and reaction rate constant were calculated according to eqn (2) and (3), respectively.

$$\text{Degradation efficiency} = \frac{C_0 - C}{C_0} \times 100\% \quad (2)$$

$$\ln\left(\frac{C_0}{C}\right) = kt \quad (3)$$

Where C_0 (mg L^{-1}) was the initial RhB solution concentration and C (mg L^{-1}) was the RhB solution concertation at the indicated time.

Cycling experiments were used to investigate the stability and reusability of the samples. The used sample was collected after the photocatalytic process as described above and was washed three times with ethanol and deionized water respectively until the washing solution was clear. The sample was then dried in a vacuum oven at 60 °C overnight for the next recycling. For powdered samples, the powders were collected by centrifugation, washed and dried, and then processed for cycling.

2.4.2 Trapping test. To determine the active species generated during the process of photocatalysis, 1 mmol L^{-1} of BQ, IPA, and EDTA-2Na were selected as scavengers and added to the photocatalytic reaction system for trapping superoxide radical ($^{\cdot}O_2^-$), hydroxyl radical ($^{\cdot}OH$) and the holes (h^+), respectively.

3. Results and discussion

3.1 Material characterization

To facilitate the nucleation and growth of MOF on a cellulose substrate, hydroxyl groups on cotton fabric were modified *via* carboxymethylation. The process involved esterification between cellulose and chloroacetate with NaOH as a catalyst.[19] As shown in Fig. 1, the broad band at 3100–3600 cm^{-1} was attributed to the –OH stretching vibration on cotton fibers. A new peak appeared at 1593 cm^{-1} corresponding to the –C=O stretching vibration, and the carboxymethyl content of CCF was determined to be 0.065 mmol g^{-1} compared to 0.000 mmol g^{-1} of CF by titration experiment, indicated the generation of carboxymethyl substituents on cotton fibers due to carboxymethylation.[20,21]

The MOF contents in the composites were determined using the weighing method (eqn (S1)†). Fig. 2 illustrated that the MOF loading decreased with an increasing amount of CTAB in the composite samples CAU-17_*X*@CCF and CAU-17_*X*@CF, which can be attributed to the competitive coordination of CTAB thus slowing down MOF nucleation time.[22,23] In addition, the loading mass of MOF on CF was significantly lower than that on CCF, demonstrating that the carboxymethylation treatment provided more MOF nucleation sites on cotton substrates. It was noticed that the calculated loading percent of CAU-17_ST@CCF/CF was negative, which was probably due to the high temperature, high pressure, and weakly acidic environment (pH = 4.2) of the reaction system during the synthesis process, which destroyed part of the cotton fibers. Additionally, cracks were observed on the surface of CAU-17_ST@CCF, and the composite fractured

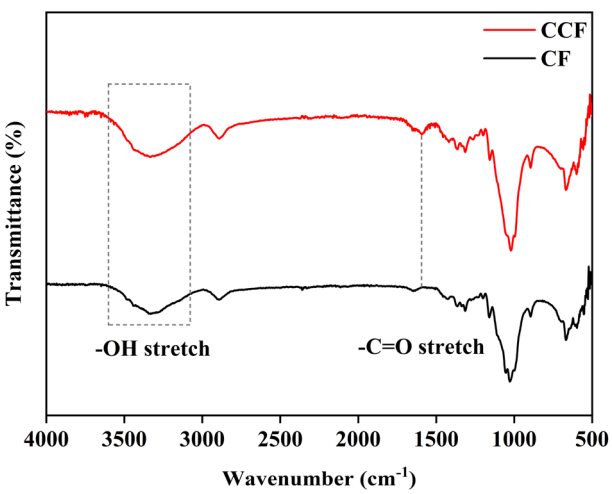

Fig. 1 FT-IR spectra of untreated CF and CCF.

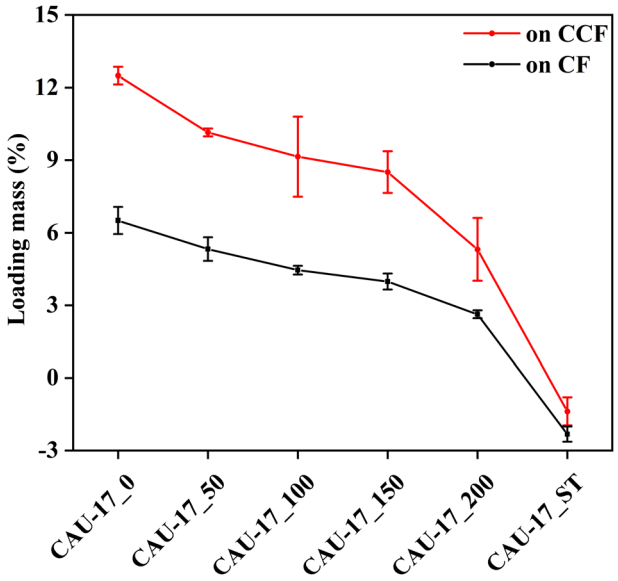

Fig. 2 Loading mass percent of CAU-17 on CCF and CF with different synthesis conditions.

under slight external force. In contrast, the ultrasonic method, with its gentler synthesis conditions, would not significantly impact the physical properties of the cotton fabrics (Fig. S1†).

XRD was utilized to confirm the MOF crystallization and the growth on CCF. In Fig. 3a, the broad diffraction peaks at 20–25° for CF and CCF indicated the crystallization of cellulose,[24] and carboxymethylation did not change the crystallization of cotton fabrics. As for the composite material CAU-17_ST@CCF and CAU-17_ST@CF, diffraction peaks belonging to CAU-17 can be observed at 7.5°, 9.9°, and 13.0°, which demonstrated that the MOF was successfully incorporated onto the cotton fabric. The weak MOF peak intensities were attributed to the low loading and the interference of the diffraction signals by the cotton fibers, consistent with previous reports on MOF-cotton materials.[25–27] Fig. 3b–d exhibited the XRD results of MOF powder and composites synthesized by the ultrasonication, respectively. As can be seen in Fig. 3b, when CTAB was not applied, the weak characteristic peak of CAU-17 and other impurity peaks were observed simultaneously in the pattern of CAU-17_0, suggesting it was a mixture with other unknown phases. After adding CTAB, the samples displayed diffraction results completely consistent with simulated CAU-17, and the amount of CTAB would not affect the crystallization. In Fig. 3c, XRD results confirmed the growth of CAU-17 on cotton fabrics by ultrasound method, which can be perfectly matched with the simulated pattern (CCDC No. 1426169).[28] Notably, the impurity peak at 11.8° disappeared until CTAB exceeded 100 mg, which was not exactly consistent with the pattern of the powder sample, suggesting that heterogeneous nucleation of precursors on cotton fabrics affects the crystallographic orientation of CAU-17. Similar results were obtained when MOF was grown on unmodified cotton fabrics, but with lower diffraction peak intensities of MOF crystals (Fig. 3d). The growth mechanism of

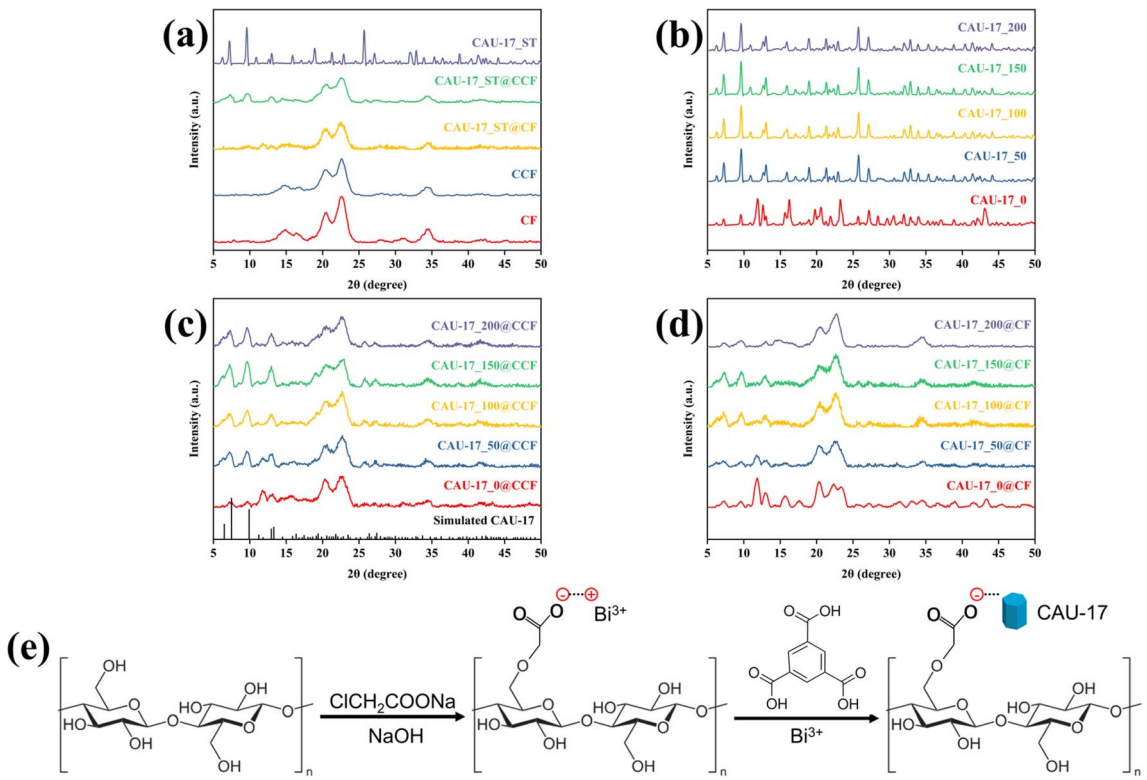

Fig. 3 XRD patterns of (a) MOF powder and cotton composite were obtained by the solvothermal route, CF, and bare CCF; (b) CAU-17_*X*; (c) CAU-17_*X*@CCF; (d) CAU-17_*X*@CF; (e) schematic of the carboxymethylation and growth of CAU-17 on CCF.

CAU-17 on cotton fibers as shown in Fig. 3e. First, more carboxyl groups were introduced to the surface of cotton fibers after carboxymethylation treatment and complexed with positively charged Bi^{3+}, subsequently CAU-17 nucleated and grew from it under suitable reaction conditions, resulting in CAU-17 crystals firmly dispersed on the surface of cotton fibers.

The microscopic morphology of the samples was examined by SEM. Fig. 4 showed the SEM images of the powdered MOF. The monodisperse CAU-17 particles exhibited typical hexagonal prism structure, and the CAU-17_*X* (length: 2.1 μm, diameter: 1.2 μm) synthesized within a short time had a smaller average size compared to CAU-17_ST (length: 4.2 μm, diameter: 0.8 μm). The concentration change of CTAB did not affect the size of the hexagonal prism particles. In addition, irregular flaky particles were present in CAU-17_0, which were considered as intermediates consistent with previous reports.[29,30]

Investigation of MOF growth on cotton fabrics by SEM. Both CF and CCF had smooth fibers (Fig. S2†), and MOF crystals were observed on the surface after in situ growth. However, as shown in Fig. S3,† the distribution of MOF on CAU-17_*X*@CF was much sparser, suggesting weak bonding between the original cotton fabric and the MOF. As for CAU-17_*X*@CCF in Fig. 5, lamellar structure was observed at low concentration of CTAB (≤100 mg), which corroborated with the XRD results; only when the CTAB was 150 mg (CAU-17_150@CCF), the uniform and dense MOF coating consisting of hexagonal prismatic crystals was obtained. Moreover, the cracks on the surface of CAU-17_100@CCF and CAU-17_150@CCF were attributed to the significant deformation of the cotton fabric during water absorption and dehydration.

The generation of lamellar structure can be attributed to the following two points: (1) the electron configuration of Bi element is $\{1s^2 2s^2 2p^6 3s^2 3p^6 4s^2 3d^{10} 4p^6 5s^2 4d^{10} 5p^6 6s^2 4f^{14} 5d^{10} 6p^3\}$, the formation of coordination bonds in the outermost 6p orbitals is usually aligned in the plane, leading to the development of layered structures.[28] (2) Compared to nucleation in a homogeneous solution, specific affinity sites on the surface of substrates (CCF) can act as nucleation directors for MOF formation and reduce the required free energy. When heterogeneous substrates are present, the affinity sites on the surface could direct the nucleation of MOF and reduce the required free energy, ultimately resulting in the formation of thermodynamically more stable intermediates.[31,32] According to previous reports,[33,34] the cationic surfactant CTAB, which has both hydrophobic and hydrophilic groups, due to the hydrocarbon long chains and quaternary ammonium cations in the structure, has been widely used as a modifier for controlling the synthesis of MOF nanocrystals. Here, the appropriate concentration of CTAB in the reaction system facilitated the establishment of nine-coordination structure between the organic ligands BTC^{3-} and Bi^{3+} corresponding to CAU-17 crystals.

XPS confirmed the surface chemical composition of MOF@CCF. Fig. 6 showed that the oxygen, carbon, and bismuth peaks were present at around 531.5, 285.0, and 162.3 eV, respectively, demonstrating the successful immobilization of Bi-MOF on cotton using various methods. The XPS high-resolution spectra of C 1s, O 1s, and Bi 4f were shown in Fig. S4,† and the samples prepared from different conditions had almost the same elemental compositional characteristics. The C 1s peaks were deconvoluted to three peaks at 284.8, 286.7, and 289.0 eV, corresponding to C–C/C=C, C–O, and O–C=O bonds, respectively.[35,36] The O 1s spectra showed three unique oxygen species, the peaks at 530.1 and 533.1 eV were associated with Bi–O bond and O in bismuth-oxo clusters of CAU-17, respectively, while the peak at 531.7 was assigned to O–H bond.[37] In the Bi 4f spectra, binding energies at 159.6 and 165.1 eV correspond to Bi $4f_{5/2}$ and Bi $4f_{7/2}$, respectively, indicating a bismuth oxidation state of +3.[38] Comparing the previous SEM results, hexagonal prism particles were found to have a higher percentage of C–O bonds than flake

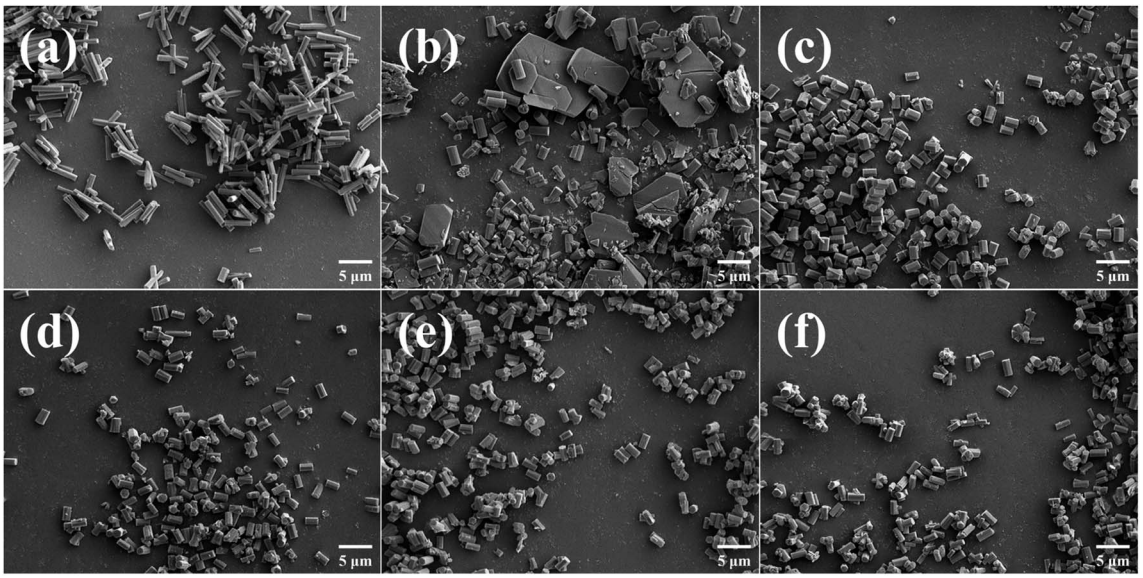

Fig. 4 SEM images of MOF powders. (a) CAU-17_ST, (b) CAU-17_0, (c) CAU-17_50, (d) CAU-17_100, (e) CAU-17_150, and (f) CAU-17_200.

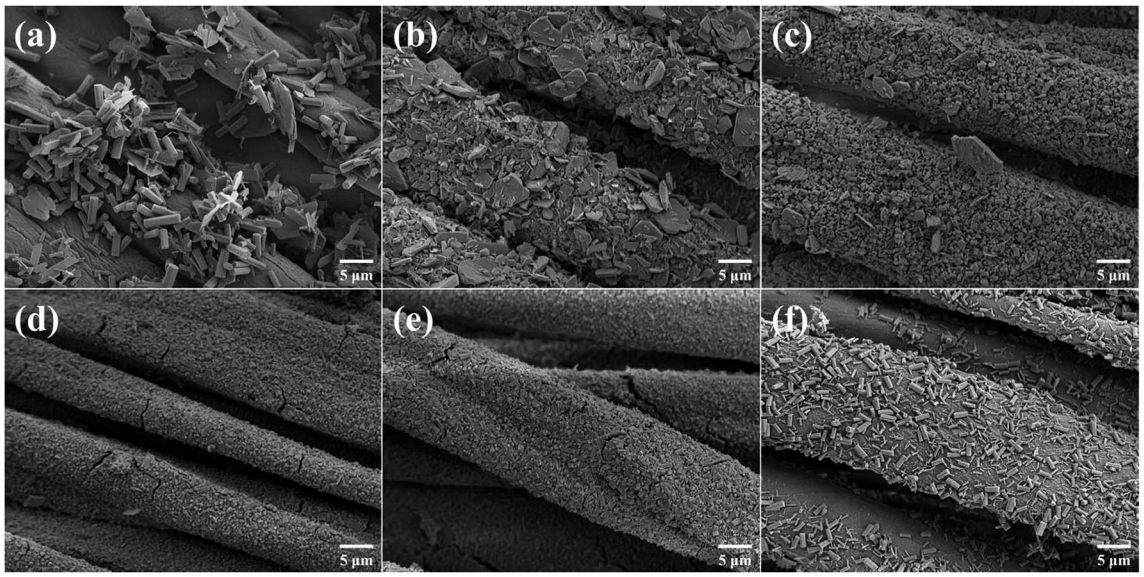

Fig. 5 SEM images of (a) CAU-17_ST@CCF, (b) CAU-17_0@CCF, (c) CAU-17_50@CCF, (d) CAU-17_100@CCF, (e) CAU-17_150@CCF, and (f) CAU-17_200@CCF.

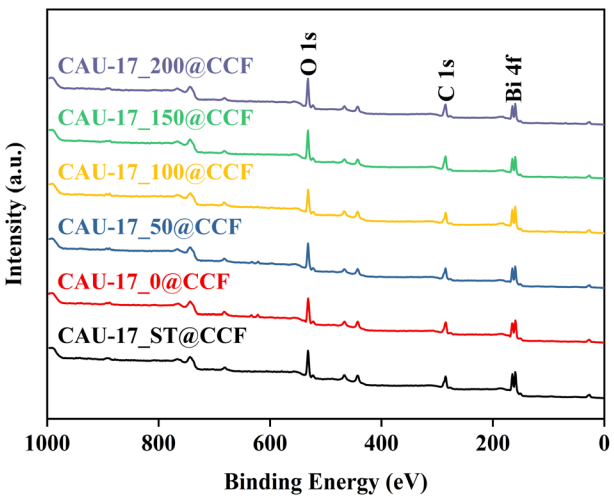

Fig. 6 XPS survey of CAU-17_*X*@CCF and CAU-17_ST@CCF.

Table 1 Pore characteristics of obtained samples

Sample	S_{BET} ($m^2\ g^{-1}$)	$V_{totalpore}$ ($cm^3\ g^{-1}$)	$V_{micropore}$ ($cm^3\ g^{-1}$)
CCF	1.160	0.001	—
CAU-17_0@CCF	9.916	0.007	0.002
CAU-17_50@CCF	18.277	0.011	0.005
CAU-17_150@CCF	20.748	0.013	0.006
CAU-17_ST@CCF	12.541	0.008	0.003
CAU-17_0	61.463	0.033	0.024
CAU-17_50	203.665	0.110	0.084
CAU-17_150	187.236	0.101	0.079
CAU-17_ST	275.428	0.144	0.119
CF	5.7167	0.013	—
CAU-17_0@CF	7.2515	0.013	—
CAU-17_50@CF	8.4829	0.013	—
CAU-17_150@CF	8.4015	0.011	—
CAU-17_ST@CF	8.7404	0.013	—

intermediates, indicating that the transformation from intermediates to the final state of CAU-17 altered the crystalline structure. Besides, the variation of the content of Bi atoms in Table S1† illustrated once again that the loading ratio of MOF on cotton fabrics was regulated by the synthesis conditions.

The pore characteristics of the obtained samples were examined using N_2 adsorption–desorption experiments, and the relevant data are presented in Table 1 for comparison. It can be seen that the carboxymethylation process would affect the pore structure of CF, resulting in a reduction in the specific surface area. The isotherms of all powder samples were classified as type I, indicating the microporous properties of the materials. Meanwhile, the specific surface area of CAU-17_0, which composed of lamellar intermediates and hexagonal prismatic particles, was only 61.463 $m^2\ g^{-1}$, indicating the intermediates were dense and nonporous structures. Fig. 7a and d revealed the diversity and abundance of pore structures in CAU-17_*X*@CCF. Mesopores were associated with the cotton fabric's structure, and the pore size predominantly fell below 2 nm, primarily attributed to the carried MOFs.[39] In addition, loading MOF onto CF did not significantly improve the specific surface area of cotton fabrics, and the micropore volume data cannot be obtained, presumably due to the low MOF loading.

Thermal analysis was carried out to explore the thermal stability. The weight loss before 120 °C can be attributed to the removal of adsorbed water for all samples. As shown in Fig. 8a and b, cotton composites exhibited mass loss in two stages: decomposition of the cotton fabric at 320 °C and collapse of the

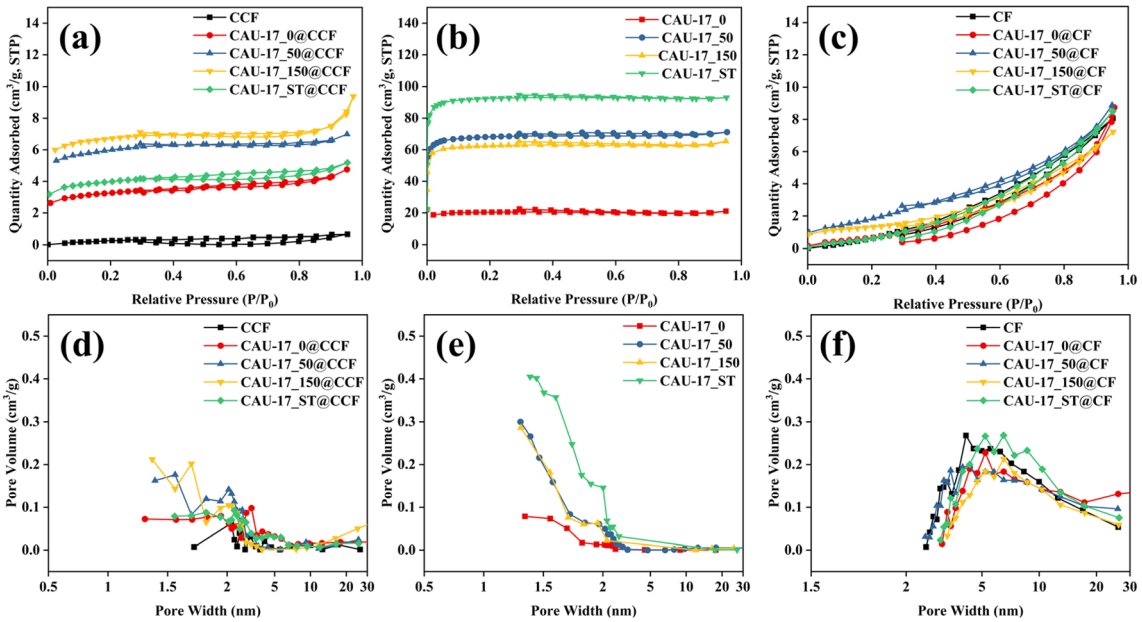

Fig. 7 N_2 adsorption–desorption isotherms and pore size distributions of (a and d) CAU-17_*X/ST*@CCF; (b and e) CAU-17_*X/ST* and (c and f) CAU-17_*X/ST*@CF.

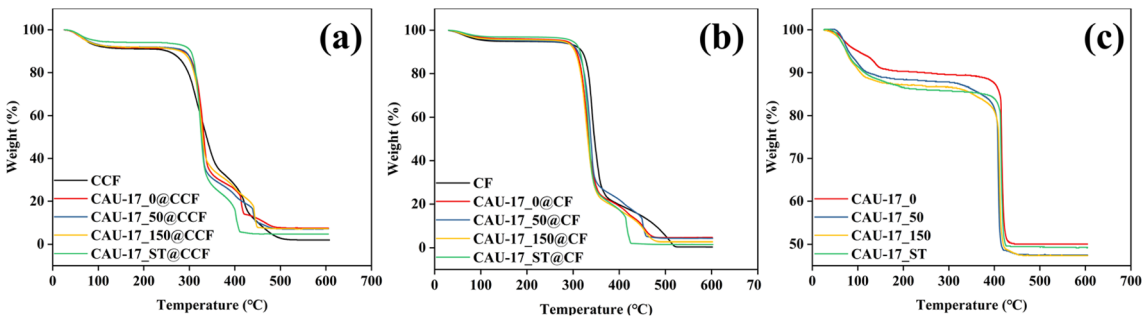

Fig. 8 TG curves of (a) CAU-17_*X/ST*@CCF; (b) CAU-17_*X/ST*@CF and (c) CAU-17_*X/ST*.

MOF structure at 410 °C. In Fig. 8c, the presence of lamellar structures does not affect the overall thermal decomposition temperature properties due to similar chemical compositions. Moreover, after temperatures exceeding 450 °C, Bi-MOF underwent conversion to Bi_2O_3 under air atmosphere.

In previous researches,[40–42] specific surface area (eqn (S2)†) and thermogravimetry (eqn (S3)†) have been recommended to calculate the loading of MOF in composites. The calculations were shown in Table 2. Comparing the two methods, it can be seen that the loadings obtained by thermogravimetry were significantly higher than those obtained by the BET method, which can be explained by the impact of the accessibility of the MOF pores for N_2 gas. Furthermore, the loading capacity of CAU-17_*X*@CF is significantly lower than that of MOF on CCF, which once again emphasized the importance of carboxymethylation treatment in improving the loading capacity of MOF on cotton substrates.

Table 2 MOF loading mass fractions calculated by BET and TG data

Sample	wt% by BET	wt% by TG
CAU-17_0@CCF	14.520	14.579
CAU-17_50@CCF	8.453	14.192
CAU-17_150@CCF	10.527	14.327
CAU-17_ST@CCF	4.150	8.546
CAU-17_0@CCF	2.753	8.557
CAU-17_50@CCF	1.397	8.214
CAU-17_150@CCF	1.479	5.100
CAU-17_ST@CCF	1.121	2.645

3.2 Photocatalytic performance

The absorbance properties of the prepared functional cotton materials were assessed using UV-vis diffuse reflectance spectra (UV-vis DRS). As depicted in Fig. 9a and c, with the addition of MOF, the photo-response range of CCF/CF was enlarged, and there was a pronounced absorption edge near the 320 nm wavelength. CAU-17_150@CCF exhibited the widest absorption range, attributed to its pure hexagonal prismatic structure and appropriate loading amount. The energy bandgap values (E_g) of

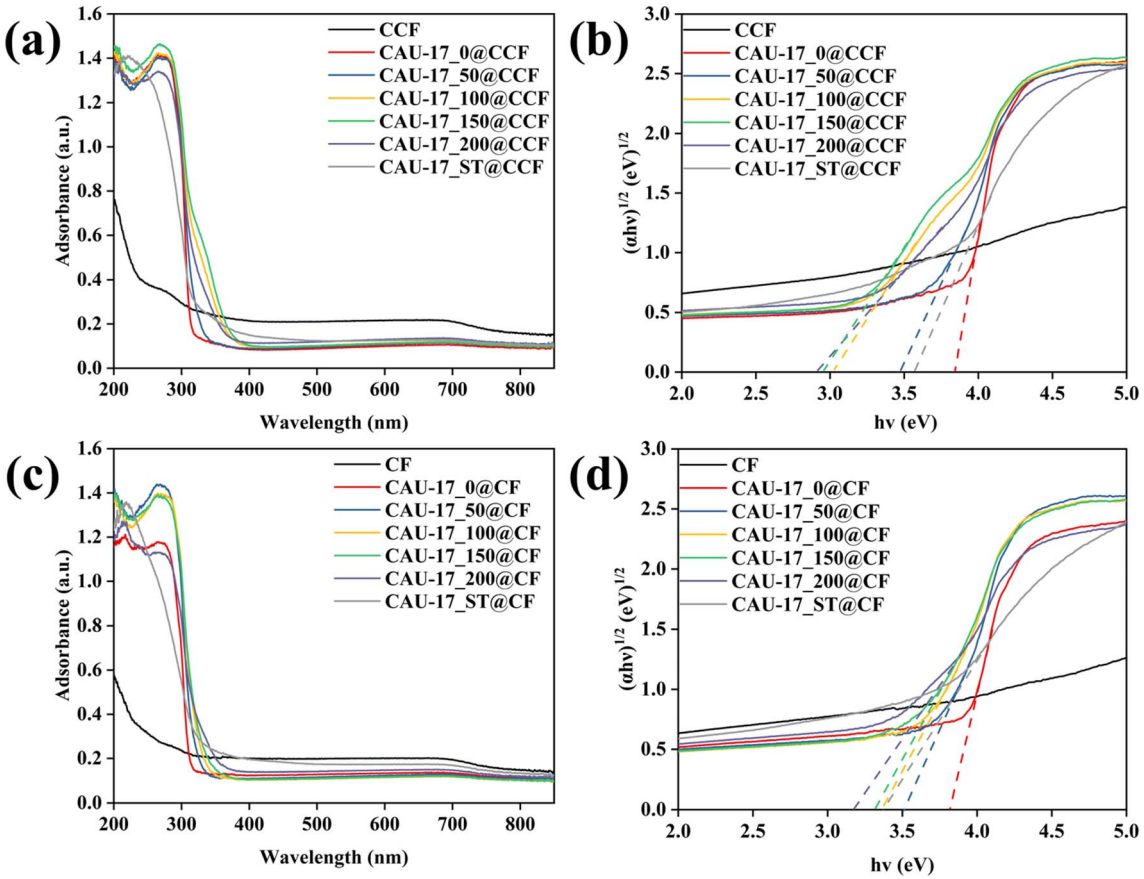

Fig. 9 (a and c) UV-vis diffuse reflectance spectra and (b and d) plots of $(\alpha hv)^{1/2}$ and the bandgap energy for CAU-17_*X/ST*@CCF and CAU-17_*X/ST*@CF, respectively.

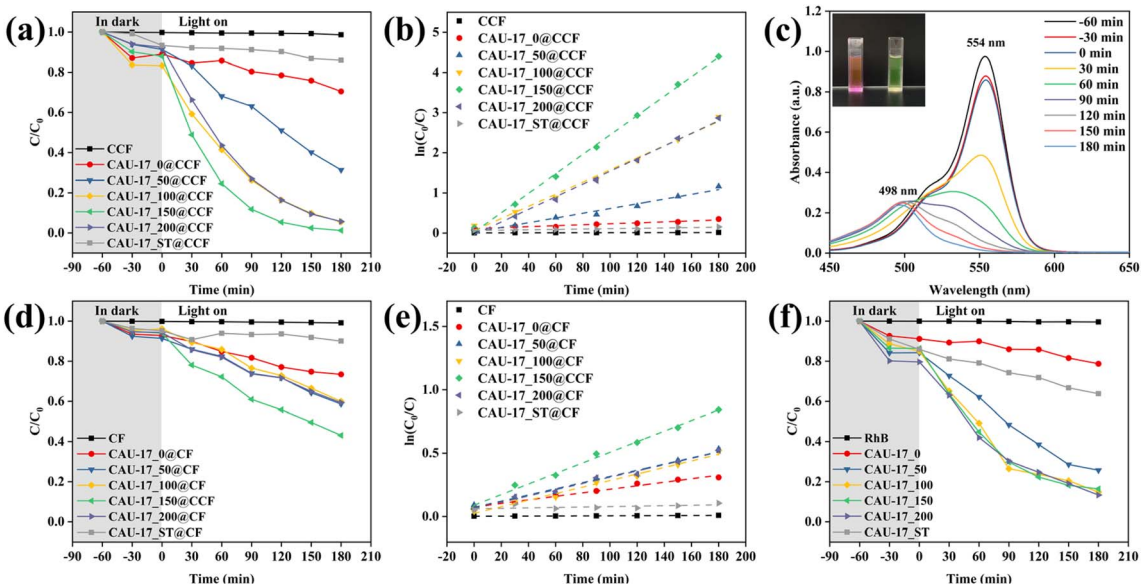

Fig. 10 (a) Photocatalytic degradation kinetics of CAU-17_*X/ST*@CCF; (b) plots for fitted kinetics modeling of CAU-17_*X/ST*@CCF; (c) UV-vis adsorption spectra of RhB solution for CAU-17_150@CCF (color change of the solution shown in the inset); (d) photocatalytic degradation kinetics of CAU-17_*X/ST*@CF; (e) plots for fitted kinetics modeling of CAU-17_*X/ST*@CF; (f) photocatalytic degradation kinetics of CAU-17_*X/ST* and pure RhB solution.

samples can be evaluated by the Tauc plot (Fig. 9b and d) with the following eqn (4):[43]

$$\alpha h\nu = A(h\nu - E_g)^{n/2} \quad (4)$$

where α, h, ν, A and n are the coefficient, Planck's constant, photon frequency, constant, and 4, respectively. The results of band gap calculations (Table S2†) indicated that the optical properties of the composite fabrics were affected by the MOF structure and loading mass, where CAU-17_150@CCF had the narrowest bandgap of 2.96 eV.

The photocatalytic performance of the samples was evaluated by using RhB dye as a pollutant model under visible light irradiation. Fig. 10a shows the variation of RhB concentration in the photocatalytic degradation reaction. Bare CCF displayed no adsorption or degradation of RhB, and MOF-loaded cotton composites reached adsorption equilibrium within the first hour. Compared with other samples, CAU-17_150@CCF presented the highest activity with a removal rate of 98.77% after 180 min of light exposure. It can be seen from Fig. 10b and Table S2† that the MOF-functionalized cotton fabrics well fitted the pseudo-first-order kinetic model and that the reaction rate constants for CAU-17_*X*@CCF were 2.6 to 52.9 times higher than that of CAU-17_ST@CCF, suggesting that smaller size hexagonal crystals were more favorable for achieving high photocatalytic performance. Fig. 10c showed the evolution of the absorption spectrum of the RhB solution in the presence of CAU-17_150@CCF over time. The intensity of the absorption peak at 554 nm gradually decreased with the increase of irradiation time, while the maximum absorption band gradually blue shifted from 554 nm to 498 nm, and the color of the RhB solution also changed from pink to light yellow. It was inferred that the photodegradation of RhB under visible light irradiation was the result of the competition between *N*-deethylation and the destruction of conjugated structure.[44,45] Moreover, comparison with the mentioned photocatalytic materials in other researches, the results are shown in Table S3,† which demonstrated that the photocatalytic performance of the samples in this work was superior among the same type of cotton composite photocatalytic materials.

For Fig. 10d and e, CAU-17_*X*@CF was set up as a control group to prove the necessity of carboxymethylation. Under the same experimental conditions, the photocatalytic performance of CAU-17_*X*@CF significantly reduced due to lower MOF content, the optimal photocatalytic efficiency could only be reached at 56.93% (CAU-17_150@CF). In addition, the photocatalytic properties of the powder samples were also investigated. As can be seen from Fig. 10f, CAU-17_50/100/150/200 showed almost identical degradation efficiencies and were significantly better than CAU-17_0/ST, which corroborated with the material characterization results mentioned. Also, it was illustrated again that the small-sized hexagonal prismatic MOF structures synthesized by ultrasonication with the assistance of CTAB have superior photocatalytic properties.

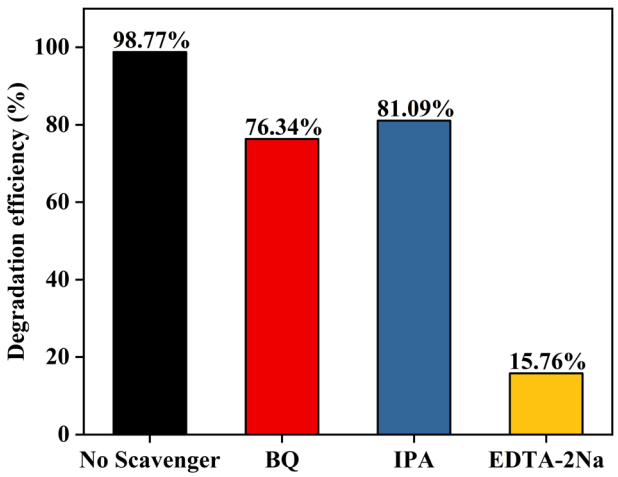

Fig. 11 Effects of different scavengers on the degradation of RhB in the presence of CAU-17_150@CCF.

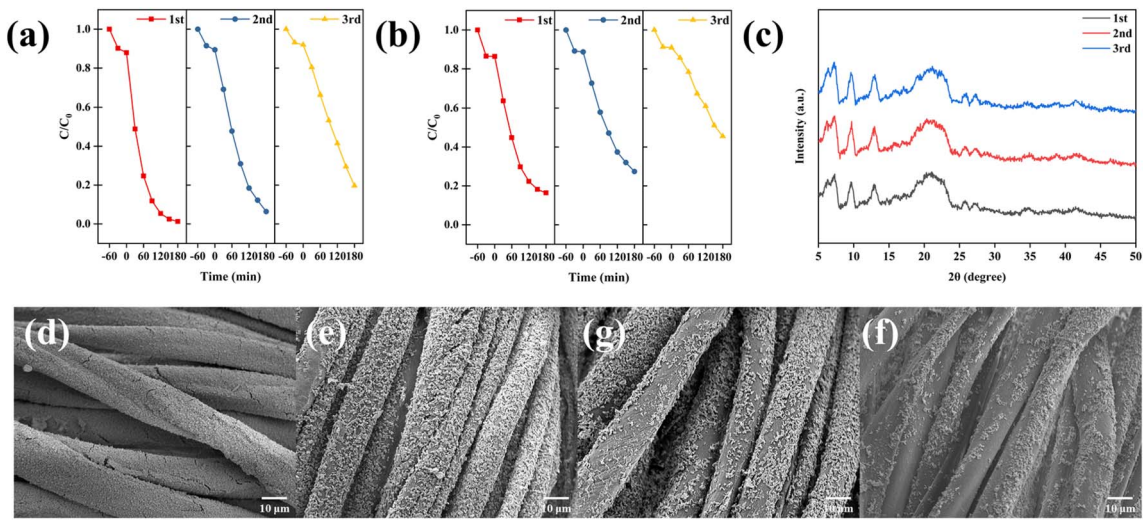

Fig. 12 Photocatalytic recycle degradation efficiency of RhB by using (a) CAU-17_150@CCF and (b) CAU-17_150; (c) XRD patterns of CAU-17_150@CCF after each recycling application; SEM images of (d) initial CAU-17_150@CCF, (e) 1st, (g) 2nd and (f) 3rd cycle.

The main active substances during the photocatalytic reaction of the samples were identified by radical trapping experiments, where BQ, IPA, and EDTA-2Na were used as scavengers of superoxide radicals ($^{\bullet}O_2^-$), hydroxyl radicals ($^{\bullet}OH$) and holes (h^+), respectively.[46] As shown in Fig. 11a, all three scavengers reduced the photocatalytic efficiency and the degradation rate was only 15.76% in the presence of EDTA–2Na, implying that all three actives contributed to the photocatalytic process, in which h^+ played a dominant role.

To examine the durability and reusability of MOF composite cotton fabrics, CAU-17_150@CCF was selected for recycling experiments (Fig. 12a). After 3 cycles, the degradation rate of 80.41% could still be maintained, while the photocatalytic efficiency of CAU-17_150 decayed more rapidly in the cycling experiments (from 83.62% in the 1st cycle to 54.51% in the 3rd cycle), which was mainly due to the unavoidable mass loss of the powdered sample during separation and collection. In Fig. 12c, XRD results of the reused samples suggested the crystal structure of CAU-17 remained stable in the aqueous system. Moreover, the SEM results (Fig. 12d–f) of CAU-17_150@CCF after cycling illustrated that some of the MOF particles were detached from the cotton fibers during the photodegradation process. Therefore, the content of Bi in the remaining solution for each cycling experiment was analyzed by ICP-AES and the results were displayed in Fig. S5.† For CAU-17_150@CCF, the residual bismuth content in the solution after each cycle was not higher than 0.025 mg mL^{-1}. Compared with the direct application of powder sample, loading MOF onto carboxymethylated cotton substrates not only facilitated the separation and collection, but also enabled most of the MOF particles to be remained in the fabric rather than being immersed in solution, which was explained by the abundance of binding sites on the carboxymethylated cotton fibers, demonstrating the cyclic stability and reusability of the prepared CAU-17_150@CCF.

4. Conclusions

In conclusion, we synthesized a functionalized textile material for visible-light photocatalytic degradation of dyes *via in situ* growth of CAU-17 on carboxymethylated cotton fabrics by room-temperature ultrasonication. Carboxymethylation treatment and room-temperature synthesis techniques are essential for increasing MOF loading and maintaining the stability of the substrate material. The dense MOF layer formed by the uniform deposition of small-sized hexagonal CAU-17 crystals on cotton fibers was verified by XRD, SEM and other analytical techniques. Subsequently, the photocatalytic performance of MOF composite cotton fabrics was explored, and the CAU-17_150@CCF synthesized under optimized conditions could achieve a degradation efficiency of 98.8% for RhB within 180 minutes under visible light irradiation. Furthermore, the composites demonstrate commendable reusability, experiencing only an 18.4% decline in catalytic efficiency after three cycles. These results indicate that the construction of functionalized cotton fabrics by *in situ* synthesis can be an attractive approach for expanding the application of Bi-MOFs, especially in the treatment of dyes in water systems.

Author contributions

Hengjie Qin: methodology, software, investigation, data curation, writing – original draft, visualization. Ying Lv: methodology, writing – review & editing. Koji Nakane: conceptualization, resources, writing – review & editing, supervision.

Conflicts of interest

There are no conflicts to declare.

Acknowledgements

The authors express their gratitude to Maeda Kosen Foundation, Japan, for partial financial support.

References

1 J. L. C. Rowsell and O. M. Yaghi, *Microporous Mesoporous Mater.*, 2004, **73**, 3–14.
2 A. J. Howarth, A. W. Peters, N. A. Vermeulen, T. C. Wang, J. T. Hupp and O. K. Farha, *Chem. Mater.*, 2017, **29**, 26–39.
3 H. Furukawa, K. E. Cordova, M. O'Keeffe and O. M. Yaghi, *Science*, 2013, **341**, 1230444.
4 Y. Li and R. T. Yang, *Langmuir*, 2007, **23**, 12937–12944.
5 Y. Peng, J. Xu, J. Xu, J. Ma, Y. Bai, S. Cao, S. Zhang and H. Pang, *Adv. Colloid Interface Sci.*, 2022, **307**, 102732.
6 Y. Wang, H. Jin, Q. Ma, K. Mo, H. Mao, A. Feldhoff, X. Cao, Y. Li, F. Pan and Z. Jiang, *Angew. Chem.*, 2020, **132**, 4395–4399.
7 Q. Wang and D. Astruc, *Chem. Rev.*, 2020, **120**, 1438–1511.
8 X. Qi, K. Liu and Z. Chang, *Chem. Eng. J.*, 2022, **441**, 135953.
9 J. Fonseca and T. Gong, *Coord. Chem. Rev.*, 2022, **462**, 214520.
10 Z. Wang, Z. Zeng, H. Wang, G. Zeng, P. Xu, R. Xiao, D. Huang, S. Chen, Y. He, C. Zhou, M. Cheng and H. Qin, *Coord. Chem. Rev.*, 2021, **439**, 213902.
11 V. H. Nguyen, T. D. Nguyen and T. Van Nguyen, *Top. Catal.*, 2020, **63**, 1109–1120.
12 G. Wang, Q. Sun, Y. Liu, B. Huang, Y. Dai, X. Zhang and X. Qin, *Chem.–Eur. J.*, 2015, **21**, 2364–2367.
13 Y.-J. Huang, Y.-Q. Zheng, H.-L. Zhu and J.-J. Wang, *J. Solid State Chem.*, 2016, **239**, 274–281.
14 Q.-X. Wang and G. Li, *Inorg. Chem. Front.*, 2021, **8**, 572–589.
15 Y. Ying, B. Khezri, J. Kosina and M. Pumera, *ChemSusChem*, 2021, **14**, 3402–3412.
16 H. N. Rubin, B. H. Neufeld and M. M. Reynolds, *ACS Appl. Mater. Interfaces*, 2018, **10**, 15189–15199.
17 H. S. Jhinjer, A. Singh, S. Bhattacharya, M. Jassal and A. K. Agrawal, *J. Hazard. Mater.*, 2021, **411**, 125056.
18 H. Ouyang, N. Chen, G. Chang, X. Zhao, Y. Sun, S. Chen, H. Zhang and D. Yang, *Angew. Chem., Int. Ed.*, 2018, **57**, 13197–13201.
19 M. da Silva Pinto, C. A. Sierra-Avila and J. P. Hinestroza, *Cellulose*, 2012, **19**, 1771–1779.

20 R. N. Wijesena, N. Tissera, R. Perera and K. M. N. de Silva, *Carbohydr. Polym.*, 2014, **109**, 56–63.
21 M. López-R, Y. Barrios, L. D. Perez, C. Y. Soto and C. Sierra, *Inorg. Chim. Acta*, 2022, **537**, 120955.
22 Y. Pan, D. Heryadi, F. Zhou, L. Zhao, G. Lestari, H. Su and Z. Lai, *CrystEngComm*, 2011, **13**, 6937–6940.
23 Q. Liu, L.-N. Jin and W.-Y. Sun, *Chem. Commun.*, 2012, **48**, 8814–8816.
24 M. López-R, Y. Barrios, L. D. Perez, C. Y. Soto and C. Sierra, *Inorg. Chim. Acta*, 2022, **537**, 120955.
25 R. Rezaee, M. Montazer, A. Mianehro and M. Mahmoudirad, *Starch/Staerke*, 2021, **73**, 2100120.
26 R. M. Abdelhameed, M. Rehan and H. E. Emam, *Carbohydr. Polym.*, 2018, **195**, 460–467.
27 M. da Silva Pinto, C. A. Sierra-Avila and J. P. Hinestroza, *Cellulose*, 2012, **19**, 1771–1779.
28 A. K. Inge, M. Köppen, J. Su, M. Feyand, H. Xu, X. Zou, M. O'Keeffe and N. Stock, *J. Am. Chem. Soc.*, 2016, **138**, 1970–1976.
29 R. Huang, Z. Zhou, X. Lan, F. K. Tang, T. Cheng, H. Sun, K. Cham-Fai Leung, X. Li and L. Jin, *Mater. Today Bio*, 2023, **18**, 100507.
30 M. Köppen, A. Dhakshinamoorthy, A. K. Inge, O. Cheung, J. Ångström, P. Mayer and N. Stock, *Eur. J. Inorg. Chem.*, 2018, **2018**, 3496–3503.
31 M. J. Van Vleet, T. Weng, X. Li and J. R. Schmidt, *Chem. Rev.*, 2018, **118**, 3681–3721.
32 G. C. Sosso, J. Chen, S. J. Cox, M. Fitzner, P. Pedevilla, A. Zen and A. Michaelides, *Chem. Rev.*, 2016, **116**, 7078–7116.
33 A. Ranft, S. B. Betzler, F. Haase and B. V. Lotsch, *CrystEngComm*, 2013, **15**, 9296–9300.
34 F. Yang, H. Mu, C. Wang, L. Xiang, K. X. Yao, L. Liu, Y. Yang, Y. Han, Y. Li and Y. Pan, *Chem. Mater.*, 2018, **30**, 3467–3473.
35 J. Jiang, Y. Xu, C. Tang, X. Wang, W. Wei and L. Ai, *Desalination*, 2023, **560**, 116680.
36 H. Jin, H.-M. Wen, Q. Hong, J. Lin, J. Li and J. Hu, *J. Mater. Chem. C*, 2022, **10**, 8310–8320.
37 X. Yue, L. Cheng, F. Li, J. Fan and Q. Xiang, *Angew. Chem.*, 2022, **134**, e202208414.
38 F. Li, G. H. Gu, C. Choi, P. Kolla, S. Hong, T.-S. Wu, Y.-L. Soo, J. Masa, S. Mukerjee, Y. Jung, J. Qiu and Z. Sun, *Appl. Catal., B*, 2020, **277**, 119241.
39 S. Q. Jabbar, H. Janani and H. Janani, *J. Polym. Environ.*, 2022, **30**, 4210–4224.
40 G. W. Peterson, D. T. Lee, H. F. Barton, T. H. Epps and G. N. Parsons, *Nat. Rev. Mater.*, 2021, **6**, 605–621.
41 M. A. Bunge, E. Pasciak, J. Choi, L. Haverhals, W. M. Reichert and T. G. Glover, *Ind. Eng. Chem. Res.*, 2020, **59**, 19285–19298.
42 A. X. Lu, M. McEntee, M. A. Browe, M. G. Hall, J. B. DeCoste and G. W. Peterson, *ACS Appl. Mater. Interfaces*, 2017, **9**, 13632–13636.
43 M.-L. Xu, X.-J. Jiang, J.-R. Li, F.-J. Wang, K. Li and X. Cheng, *ACS Appl. Mater. Interfaces*, 2021, **13**, 56171–56180.
44 J. Zhang and Z. Ma, *RSC Adv.*, 2017, **7**, 2163–2171.
45 J. Xia, S. Yin, H. Li, H. Xu, L. Xu and Y. Xu, *Dalton Trans.*, 2011, **40**, 5249–5258.
46 F. Yu, F. Gong, Q. Yang and Y. Wang, *Diamond Relat. Mater.*, 2022, **125**, 109004.